Physica B 432 (2014) 116–120

Contents lists available at ScienceDirect

Physica B

journal homepage: www.elsevier.com/locate/physb

Unexpected features of the formation of Si and Ge nanocrystals during annealing of implanted SiO_2 layers: Low frequency Raman spectroscopic characterization

Venu Mankad [a], N.N. Ovsyuk [b], Sanjeev K. Gupta [a], Prafulla K. Jha [a,*]

[a] Department of Physics, Maharaja Krishnakumarsinhji Bhavnagar University, Bhavnagar 364001, India
[b] Institute for Geology and Mineralogy, Siberian Branch, Russian Academy of Sciences, Novosibirsk 630090, Russia

ARTICLE INFO

Article history:
Received 31 August 2013
Received in revised form
17 September 2013
Accepted 20 September 2013
Available online 27 September 2013

Keywords:
Semiconductors
Ion-implantation
Raman-spectroscopy
Acoustical properties

ABSTRACT

The present paper reports a study of the influence of heat treatments on the ion-beam synthesis of Si and Ge nanocrystals in SiO_2 layers by low-frequency Raman scattering. Low-frequency Raman scattering is used just because the appearance in the glass matrix of crystal nuclei leads to an additional contribution to the density of only low-frequency acoustic vibrational states due to surface vibration modes of the nuclei. Electron microscopy, contrary to expectations, revealed a decrease rather than increase in the size of the crystal nucleus during annealing. Additionally, low-frequency Raman spectra show that the samples do not have a smooth distribution of nanoparticle sizes, as expected, but two different sizes of Si and Ge nanocrystals. This similarity is surprising because Si and Ge have different diffusion coefficients, temperatures of crystallization, meltings, and binding energies. Despite this, in both cases the same mechanism operates during the growth of Si and Ge nanocrystals.

1. Introduction

Silicon and germanium nanocrystals embedded in a dielectric matrix have attracted great interest over the last few years for their important physical and chemical properties [1–12]. The main properties of these materials are related to the confinement of (quasi)particles (electrons, holes, phonons, excitons, etc.) in volume corresponding to the radii on the order of nanometers. A strong correlation between the particle size and the band gap has been established. For this reason, the essential requirement for different applications of Si and Ge nanoparticles is to have an accurate knowledge of the particle size, size distribution and particle growth. Simultaneous control of nanoparticles size and composition will extend the range of applications of nanoparticles/glass systems. In the past decade, there has been much interest in the vibrational properties of semiconductor nanoparticles as the emission of phonon is one of the most important electronic dephasing mechanisms. Particle sizes and surface structures have been shown to be the most important factors that decide optical properties and light emitting efficiencies of these nanostructure materials. Apart from modifying the electronic structure, the spatial confinement also alters the electron–phonon coupling, an important component to determine the Raman intensity. The acoustic phonon sidebands encountered in the photoluminescence (PL) are found to affect energy relaxation in nanoparticles. The modification resulting into the phonon spectra mainly in the low frequency region from confinement resulted in a new field of nanoscale science, known as phonon engineering or nanophononics [13]. Reducing the size of electronic devices below the acoustic phonon mean free path gives new possibilities for phonon propagation and interaction. Raman scattering probes the vibrational states of the particles such as the confined acoustic, optical and surface phonon modes and provides an understanding of electron–phonon interactions. This has led to several investigations of acoustic vibrations of spherical nanoparticles, particularly the semiconductor nanoparticles leading to an understanding of the role of vibrations in the performance of some optical devices (for example, in electronic dephasing due to emission of phonons) [14,15]. Low-frequency Raman scattering caused by interaction of visible light with acoustic vibrational modes of nanocrystals has been used to study the particle size distribution and the coupling between the particle and matrix according to the vibrational theories of acoustic phonons confined in nanoparticles [16–22]. This is because of the fact that in nanoparticles due to violation of the wave vector conservation rule, the total density of vibrational states is observed in Raman scattering spectra. This feature allows one to study the initial stage of crystallization since the occurrence of crystal nuclei in a matrix of glass results in an additional contribution to density of the acoustic vibrational states associated with the surface vibrational modes of nanocrystals. More than 100 years ago, Lamb [16] discussed the

* Corresponding author. Tel.: +91 278 2422650; fax: +91 278 2426706.
E-mail addresses: prafullaj@yahoo.com, pkj@bhavuni.edu (P.K. Jha).

0921-4526/$ - see front matter © 2013 Elsevier B.V. All rights reserved.
http://dx.doi.org/10.1016/j.physb.2013.09.044

vibrations of a homogenous spherical elastic body under stress-free boundary conditions. This provided sufficiently good agreement to confirm that confined acoustic phonon modes were really being observed. The nanoparticle vibrations can be classified by their angular momentum number $l \geq 0$ and its z component m (m=azimuthal quantum number). The vibrational modes can be classified either as spheroidal or torsional. The torsional mode frequencies depend on the transverse acoustic phonon velocity v_t, while the spheroidal mode frequencies depend on both the longitudinal and transverse acoustic phonon velocity v_l and v_t respectively. The observation of these modes requires polarization measurements, since spherical vibrations lead to a polarized scattering, while the torsional vibrations bring about a depolarized scattering. It has been established [17] that only the lowest energy spheroidal modes with l equal to 0 and 2 are Raman active. The glass matrix influences the eigen-frequencies of the surface vibrational modes of nanocrystals [18]. To understand the crystallization of nanoparticles in glass matrix, modified models based on Lamb's theory such as complex frequency [12,14,19–22] and core–shell models [12,20–23] can be used which are quite successful in the interpretation of acoustic modes of nanoparticles embedded in medium.

In the present paper, we present an analysis of the formation of the most important group IV semiconductor nanocrystals such as Si and Ge glass matrix which has attracted much interest because of their potential applications in Si based optoelectronics, nanophotonics and electronic/optical memory devices. Further, interest to study the low frequency Raman scattering in these two semiconductors is due to the fact that the Ge nanocrystals show stronger confinement effect [23] resulting from direct gap semiconductor nature [24] in contrast to Si nanocrystals. This may be useful in understanding the formation of two different types of nanocrystals in different hosts. Out of several techniques to form nanocrystals of Si and Ge like doping of nanocrystals [25,26], use of pulsed heat treatments [27], introduction of additional precipitation centers [28,29], etc., the ion implantation technique is another possible method for the formation of nanocrystals. However, there is a requirement of intermediate heat treatments to form nanocrystals using ion implantation and in clarifying the mechanism of their formation [30–33]. It will be seen in what follows that the same mechanism operates even during the growth of Si and Ge nanocrystals.

2. Samples and experimental details

Silicon and germanium nanocrystals are prepared using implantation of Si^+ and Ge^+ ions at room temperature on SiO_2 films of 0.6 μm thickness with the dose of $\sim 10^{17}$ cm^{-2} [30] and energy in the range of 140–150 keV. It has been found that Si and Ge clusters are formed immediately after implantation. Si^+ implanted SiO_2 layers have been heat treated at 1100 °C. However, the annealing has been carried out within 30 min for Si NCs. Evolution of Si and Ge NCs has been studied using low frequency Raman scattering and optical Raman spectra. Some preliminary results are presented elsewhere [33]. Raman spectra were recorded at room temperature in the backscattering geometry with vertically polarized 532 nm laser. Scattered light from the samples is dispersed using a double monochromator (Spex, model 14018) and detected using a photomultiplier tube ITT FW-130 operating in the photon-counting mode. Scanning of the spectra and data acquisition was carried out using a microprocessor based data-acquisition-cum-control system. Low frequency Raman spectra have been recorded from 5 to 50 cm^{-1} at steps of 0.5 cm^{-1} while optical Raman spectra were recorded in the range of 40–1500 cm^{-1} using the same Raman spectrometer. Raman scattering experiments have been carried out on the samples placed in vacuum to eliminate air lines during recording of the low frequency spectra. The spectra have been recorded several times under the same conditions and data have been accumulated in order to detect less intense lines and to improve the signal to noise ratio. In order to fit the measured Raman spectra first the exponential background is subtracted from the observed data to remove the Rayleigh background in Figs. 2 and 3. This is followed by a straight line subtraction for the appearance of modes. After subtraction, the resulting spectrum is deconvoluted by Lorentzian contours using a peak fit process, i.e., by PEAKFIT software. The correctness of the process is confirmed by the final fitted spectrum (full curve in figure) passing through the observed data and most importantly is the resultant of the addition of all peaks under the fitted curve. The morphology of the NCs was characterized by a high resolution electron microscope (Fig. 1).

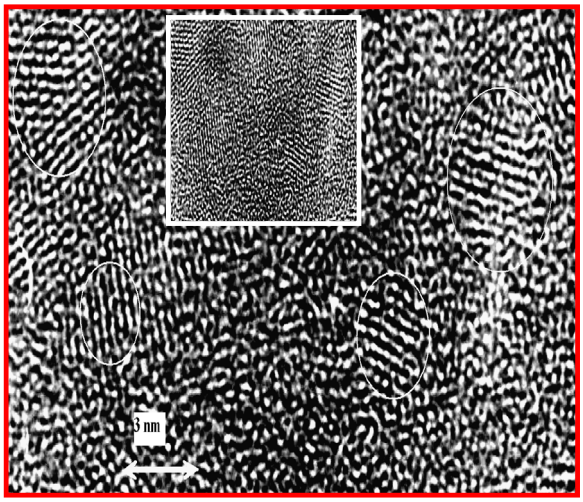

Fig. 1. Images of transverse sections of the sample after annealing at 1100 °C for Si nanoparticles. Lattice fringes corresponding to the {1 1 1} planes of Si can be clearly seen which are encircled. Two nanocrystals with a diamter of about 3 nm and 6 nm are shown.

3. Results and discussion

Experiments were conducted to study the structure of nanocrystals with high-resolution transmission electron microscopy. Fig. 1 shows a typical electron micrograph of Si nanocrystals embedded in a SiO_2 matrix. We can clearly see lattice fringes corresponding to the {1 1 1} planes of Si nanocrystals. According to electron diffraction, the interlayer distance is 0.314 nm, which corresponds to silicon, while for germanium this distance is greater and equal to 0.327 nm. It is found that each Si nanocrystal is a single crystal with good crystallinity and they are well dispersed in SiO_2 matrices. From this micrograph, we can observe two average sizes of Si nanocrystals of 3 nm and 6 nm. A TEM micrograph where only Si NPs with single sized particle is observed, a figure of interest, is shown in Fig. 1 of Ref. [33]. Figs. 2 and 3 respectively depict the low frequency Raman spectrum of Si and Ge NCs embedded in SiO_2. Both spectra show the presence of two peaks which are caused by the interaction of visible light with the acoustic vibrational modes of nanocrystals. These two peaks which correspond to the particle of two different sizes are due to the spheriodal mode with angular momentum $l=0$ and index $n=0$ (symmetric mode) as the peaks are recorded with polarized scattering. In the case of polarized Raman scattering the field vector of the exciting and scattered waves is parallel to the scattering plane, while the other Raman active spheroidal mode $l=2$ (quadrupolar mode) provides depolarized spectra. Fig. 2(a) shows that the two peaks due to spheroidal

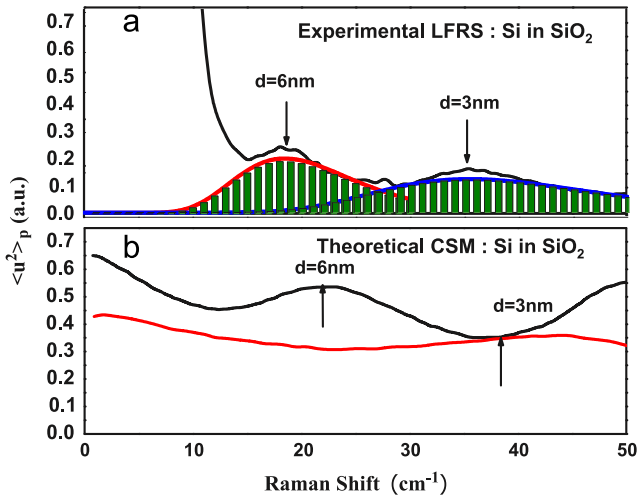

Fig. 2. (a) Low-frequency Raman spectrum of Si nanocrystals in SiO_2 layers formed after implantation and annealing for 30 min at 1100 °C. (b) Spheroidal mode $l=0$ for Si nanocrystal in SiO_2 matrix using core–shell model for the Si nanoparticles of two different sizes.

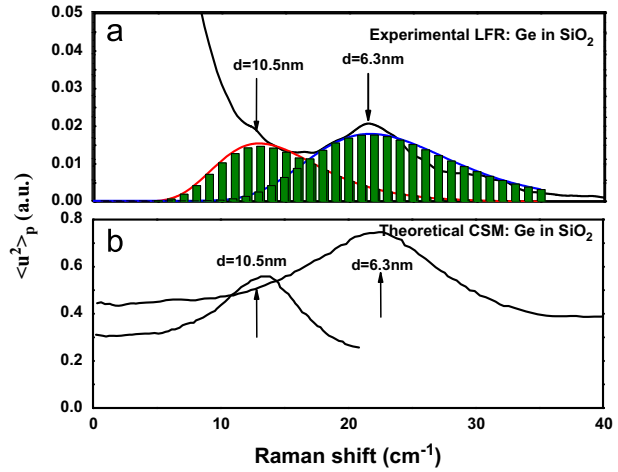

Fig. 3. (a) Low-frequency Raman spectrum of Ge nanocrystals in SiO_2 layers. (b) Spheroidal mode $l=0$ for Ge nanocrystal in SiO_2 matrix using core–shell model for Ge nanoparticles of two different sizes.

symmetric mode occuring at 18.5 and 35 cm^{-1} corresponding to 6.0 and 3.0 nm for Si particles respectively. However, for Ge nanoparticles the $l=0$ spheroidal symmetric mode occurs at 13 and 22 cm^{-1} corresponding to 10.5 and 6.3 nm sizes respectively (Fig. 3(a)). This is due to the fact that annealing is carried out at an intermediate step of 30 min, which seems to result in incomplete transformation from a loosely packed cluster of 6 nm to precipitates of 3 nm and hence the existence of nanocrystals of two sizes in the same samples is observed. Low-frequency Raman spectra show that the samples do not have smooth distribution of nanoparticle size as expected, but have two different sizes of nanoparticles. The full width at half maxima (FWHM) of these peaks indicate the size distribution of Si and Ge clusters. Figs. 2(b) and 3(b) present the mean square displacement $\langle u^2\rangle_p$ of Si and Ge nanoparticles respectively. $\langle u^2\rangle_p$ is the measure of internal motion of the nanoparticles and the approach is generally known as the core–shell model [22].

The mean square displacement can be compared to the Raman spectra, as the Raman intensity depends on the square of displacement. Moreover, the Raman intensity is governed by both $\langle u^2\rangle_p$ and the electron–phonon interaction of matrix element. The matrix element determines the overall intensity while $\langle u^2\rangle_p$ determines both amplitude and the spectral lineshape. The low frequency peak can be well simulated by a log-normal distribution with the following expression:

$$I(\omega)=\frac{1}{(2\pi)^{1/2}\ln\sigma}\,e^{-(\ln\omega-\ln\bar{\omega})/2\ln^2\sigma} \quad (1)$$

where $\bar{\omega}$ is the most probable ω and σ is the standard deviation. The standard deviation is slightly above 1 for particles of all sizes present in Si and Ge nanoparticles. Since each particle vibrates with a frequency that is inversely proportional to its size (diameter) D, the density of vibrational states $g(\upsilon)$ corresponds to the size distribution $N(D)$. This suggests that the intensity fitted from Eq. (1) to the peaks in low frequency Raman spectra corresponds to the usual size distribution, and parameter σ measures the size distribution as mentioned above. The most common size distributions encountered in different nanomaterials can be well approximated with Gaussian distribution or log-normal distribution functions. However, we use here the log-normal distribution functions. The Raman scattering technique to find the size distribution can be a complementary technique to transmission electron microscopy (TEM) and X-ray scattering. TEM and X-ray have some limitations despite being commonly used and accurate. While TEM needs expensive electron microscopes, the Debye–Scherrer formula which is used to calculate the size distribution in X-ray scattering is precisely for the case of very narrow size distribution [34].

The peak at about 35 cm^{-1} in low frequency Raman spectra corresponding to the size 3 nm of Si nanoparticles has a broader line shape. This is due to the fact that the surface effect increases with the decrease in nanocrystalline size and results in strong surface vibrational modes. In addition, there is an effect from interaction between particles and SiO_2 layer. The electron micrograph shows that the average size of precipitates decreases from ~(4–5) to ~(3–4) nm [30]. This decrease is caused by high probability of nucleation in all the modes of implantation and annealing used in this study. The optical Raman scattering and photoluminescence data show that the Si nanocrystals are of different sizes [31]. The transmission electron micrograph for Ge is similar and is not shown here. The peak at ~22 cm^{-1} corresponds to smaller sized particles of 6.3 nm with larger size distribution for Ge nanocrystals. However, it is important to note that electron microscopy, contrary to expectations, revealed a decrease rather than increase in the size of the crystal nucleus during annealing. It is known that with increasing annealing temperature, the size of nanocrystals grows usually. Therefore, low frequency Raman spectra show that samples do not have a smooth distribution of nanoparticle size as expected but consist of two different sizes of nanoparticles. This is surprising also because Si and Ge have different diffusion coefficients, temperatures of crystallization, meltings and binding energies. However, in both cases the same mechanism operates during the growth of nanoparticles and in the end one obtains two different nanoparticle sizes of 3 and 6 nm for Si and 6 and 10 nm for Ge. The reason for Ge nanocrystals being larger than Si, despite the same implantation dose, can be attributed to the fact that the concentration of germanium is two times more due to higher relative density and diffusion length for Ge is shorter than that of Si.

To verify the presence of particles of two different sizes and formation of nanoparticles in steps, the Raman shift obtained from low frequency Raman spectra can be verified from eigen-frequency calculations. Low-frequency Raman peaks in nanocrystalline materials, ascribed to confined acoustic phonon like vibrations, can be well interpreted from the different variants of original Lamb's model [16]. In the present study, we have performed the calculation of low frequency Raman spectra using all three approaches, Lamb's model, CFM and CSM, and compared them with experimental Raman shift obtained from the low frequency Raman experiment corresponding to nanoparticles of

Table 1
Low frequency Raman frequencies for Si and Ge nanoparticles embedded in SiO_2 glass.

Sample	Size d_{LFR} nm	Lamb calculation $l=0$ (cm^{-1})	CSM $l=0$ (cm^{-1})	CFM (cm^{-1})	Expt (cm^{-1})
Si/SiO_2	6	20.036	22.0	18.3	18.4
	3	40.072	38.3	36.7	35.7
Ge/SiO_2	10.0	12.9	13.5	15.5	13.1
	6.0	21.6	22.3	25.9	21.5

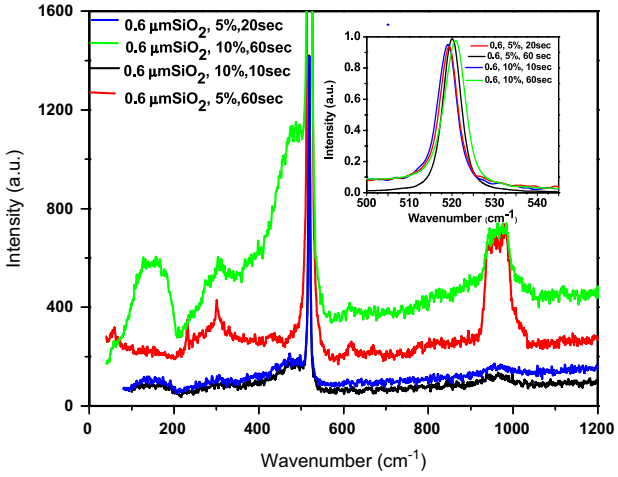

Fig. 4. Optical Raman spectra for Si nanocrystal embedded in SiO_2.

two sizes for Si and Ge nanoparticles (Table 1). To calculate the eigen-frequencies of the Si and Ge nanocrystals in SiO_2 matrix, following values of the parameters are used: $\rho_{Si}=2.33$ g/cm^3, $\nu_l(Si)=9.01\times10^5$ cm/s, $\nu_t(Si)=5.37\times10^5$ cm/s, $\rho_{SiO_2}=2.2$ g/cm^3, $\nu_l(SiO_2)=5.95\times10^5$ cm/s, $\nu_t(SiO_2)=3.76\times10^5$ cm/s, $\rho_{Ge}=5.33$ g/cm^3, $\nu_l(Ge)=5.25\times10^5$ cm/s, and $\nu_t(Ge)=3.25\times10^5$ cm/s. All methods are in good agreement and they compared well with the experiment. The lower panel of Figs. 2 and 3 presents the low frequency spectra of symmetrical mode for the nanoparticles of both sizes using CSM. It is observed that the interaction of nanocrystals with the matrix broadens and shifts the lines, but this shift is much smaller than is expected. It is remarkable and surprising to note that the mechanism of growth is the same in both Si and Ge nanocrystals despite having different physical parameters such as temperature, diffusion coefficients, temperature of crystallization, melting and binding energy for both compounds. Additionally, low frequency Raman spectra show that samples do not have a smooth distribution of nanoparticle sizes as expected but have two different sizes of Si and Ge nanocrystals.

Now turning our attention towards optical phonon Raman spectra and a new mode arising in the Si nanoparticles at about 145 cm^{-1} (Fig. 4) first we consider the mode at 145 cm^{-1} in the case of Si NCs as the said mode is observed only in the case of Si NPs, and later the complete optical spectra. It is attributed to disorder activated transverse acoustical scattering of first order arising due to the relaxation or breakdown in the wave vector selection rule, a likely event in the case of disordered materials, or finite size effect [35] confirmed from TEM image. To confirm the phonon confinement effects in the Si clusters the Raman spectra can be recorded with different laser outputs and exposure times. Fig. 4 presents the first order optical band to the samples with different exposure times and different laser power spots for Si nanocrystals. It shows clearly a fingerprint of Si crystallinity and a slight shift as expected for phonon confinement and strain effect. While compressive strain leads to an upwards shift of the Si–Si mode ($\sim$520 cm^{-1}), the phonon confinement leads to a downward shift [35]. The spectrum depicts the first order long wavelength optical band along with other features such as second order acoustical and optical band centers near 306 and 966 cm^{-1} respectively. These can be attributed to phonon density of states with a scale multiplied by 2. In the inset of Fig. 4, we present the enlarged spectrum centered at main peak 520 cm^{-1}. It is hence seen from the figure that the decrease in exposure time and laser power results in downward shift (blue-shift) of 520 cm^{-1}peak. This indicates that more laser power or more exposure time results in the strain and confinement effects together. Similar conclusions are drawn for Ge nanocrystals.

4. Conclusion

In conclusion by carefully examining the low frequency Raman spectra and theoretical calculations we have adequately explained the formation of Si and Ge nanocrystals in SiO_2 layers synthesized by the ion implantation of Si and Ge ions respectively with intermediate heat treatments. The occurrence of crystal nuclei in a matrix of glass results in an additional contribution to density of the acoustic vibrational states associated with the surface vibrational modes of nanocrystals. Unexpectedly, electron microscopy showed a decrease rather than increase in the size of the nuclei during annealing. It is apparent that the Si and Ge atoms are precipitated preferentially on the newly formed nucleus of silicon in the course of the heat treatments. Low frequency Raman scattering caused by interaction of visible light with acoustic vibrational modes of nanocrystals is an effective method of researching it and confirms that loosely packed clusters of larger size are completely transformed into compact, separate phase nanoscale precipitates of Si and Ge annealing. We observe from the low frequency Raman spectra that there is no smooth distribution of nanoparticles sizes as expected; rather two different sizes of silicon and germanium nanocrystals are observed. This is in contrast to general expectation as Si and Ge have different diffusion coefficients, temperatures of crystallization, meltings and binding energies. This indicates that the same mechanism operates during the growth of Si and Ge nanocrystals. The size distribution has been also calculated using low frequency Raman spectra and it is found that the size distribution is very narrow for both nanocrystals. We also discussed the advantage of low frequency Raman spectra to find the size distribution. A low frequency peak is observed in the optical Raman spectra of Si nanocrystals due to disorder activated transverse acoustical scattering of first order arising from the relaxation of breakdown of the wave vector selection rule. The increase in laser power or exposure time results in strain as well as confinement effects in the case of nanoparticles.

Acknowledgment

The authors are grateful to G.A. Kachurin for preparation of the samples. Authors are thankful to the Department of Science and Technology, (DST), Government of India and the Russian Foundation for Basic Research (Grant no. 11-02-92716) for the financial assistance.

References

[1] M. Ehbrecht, H. Ferkel, F. Huisken, L. Holz, Y.N. Polivanov, V.V. Smirnov, O.M. Steimakh, R. Schmidt, J. Appl. Phys. 78 (1995) 5302.
[2] M. Ehbrecht, B. Kohn, F. Huisken, M.A. Laguna, V. Paillard, Phys. Rev. B 56 (1997) 6958.

[3] H. Xia, Y.L. He, L.C. Wang, W. Hang, X.N. Liu, X.K. Zhang, D. Fang, H.E. Jackson, J. Appl. Phys. 78 (1995) 6705.
[4] W. Cheng, S.F. Ren, Phys. Rev. B 65 (2002) 205305.
[5] T. Seto, T. Orii, M. Hirasawa, N. Aya, Thin Solid Films 437 (2003) 230.
[6] Y. Xia, P Yang, Adv. Mater. 15 (2003) 353.
[7] Y. Cui, Q. Wei, H. Park, C.M. Lieber, Science 293 (2001) 1289.
[8] S. Tiwari, F. Rana, H. Hanafi, A. Hartstein, E.F. Crabbè, K. Chan, Appl. Phys. Lett. 68 (1996) 1377.
[9] W.K. Choi, W.K. Chim, C.L. Heng, L.W. Teo, V. Ho, V. Ng, D.A. Antoniadis, E.A. Fitzgerald, Appl. Phys. Lett. 80 (2002) 2014.
[10] G. Conibeer, M. Green, E.C. Cho, D. Konig, Y.H. Cho, T. Fangsuwannarak, G. Scardera, E. Pink, Y. Huang, T. Puzzer, Thin Solid Films 516 (2008) 6748.
[11] A.I. Ekimov, A.A. Onuschchenko, JETP Lett. 40 (1984) 1136.
[12] M. Talati, P.K. Jha, Phys. Rev. E 73 (2006) 011901;
M. Talati, P.K. Jha, Phys. Rev. E 77 (2008) 029904.
[13] A. Balandin, J. Nanosci. Nanotechnol. 5 (2005) 1015.
[14] V.A. Dubrovskiy, V.S. Morochnik, Izv. Earth Phys. 17 (1981) 494.
[15] A.I. Ekimov, A.A. Onuschchenko, JETP Lett. 34 (1981) 345.
[16] H. Lamb, Proc. London Math. Soc. 13 (1882) 187.
[17] E. Duval, A. Boukenter, B. Champagnon, Phys. Rev. Lett. 56 (1986) 2052.
[18] N.N. Ovsyuk, V.N. Novikov, Phys. Rev. B 53 (1996) 3113.
[19] S.K. Gupta, P.K. Jha, A.K. Arora, J. Appl. Phys. 103 (2008) 124307;
S.K. Gupta, S. Sahoo, P.K. Jha, A.K. Arora, Y.M. Azhniuk, J. Appl. Phys. 106 (2009) 024307.
[20] L. Saviot, D.B. Murray, M.C. Marco de Lucas, Phys. Rev. B 69 (2004) 113402.
[21] P. Verma, W. Cordts, G. Irmer, J. Monecke, Phys. Rev. B 60 (1999) 5778.
[22] D.B. Murray, L. Saviot, Phys. Rev. B 69 (2004) 094305.
[23] A. Tamura, K. Higeta, T. Ichinokawa, J. Phys. C: Solid State Phys. 15 (1982) 4975.
[24] C. Bostedt, T. van Burren, T.M. Willey, N. Franco, L.J. Terminello, C. Heske, T. Moller, Appl. Phys. Lett. 84 (2004) 4056.
[25] J.R. Heath, J.J. Shiang, A.P. Alivisatos, J. Chem. Phys. 101 (1994) 1607.
[26] A. Mimura, M. Fujii, S. Hayashi, et al., Phys. Rev. B 62 (2000) 12625.
[27] G.A. Kachurin, S.G. Yanovskaya, D.I. Tetel'baum, A.N. Mikhaĭlov, Fiz. Tekh. Poluprovodn. (St. Petersburg) 37 (2003) 738;
G.A. Kachurin, K.S. Zhuravlev, N.A. Pazdnikov, et al., Nucl. Instrum. Methods Phys. Res. B 583 (1997) 583.
[28] J. Zhao, D.S. Mao, Z.X. Lin, et al., Appl. Phys. Lett. 74 (1999) 1403.
[29] G.A. Kachurin, S.G. Yanovskaya, K.S. Zhuravlev, M.O. Ruault, Fiz. Tekh. Poluprovodn. (St. Petersburg) 35 (2001) 1235;
G.A. Kachurin, S.G. Yanovskaya, K.S. Zhuravlev, M.O. Ruault, Semiconductors 35 (2001) 1182.
[30] G.A. Kachurin, V.A. Volodin, D.I. Tetel'baum, D.V. Marin, A.F. Leĭer, A.K. Gutakovskiĭ, A.G. Cherkov, A.N. Mikhaĭlov, Semiconductors 39 (2005) 552.
[31] B.G. Potters, J.H. Simmons, Phys. Rev. B 37 (1988) 10838.
[32] Y. Maeda, Phys. Rev. B 51 (1995) 1658.
[33] N.N. Ovsyuk, V. Mankad, S.K. Gupta, P.K. Jha, G.A. Kachurin, in: Proceedings of the 2nd International Conference on Low Dimensional Systems (LDS-2), Bull. Russ. Acad. Sci. Phys. 75 (2011) 601.
[34] (a) M. Ivanda, K. Babocsi, C. Dem, M. Schmitt, M. Montagna, W. Kiefer, Phys. Rev. B 67 (2003) 235329;
(b) M. Ivanda, A. Hohl, M. Montagna, G. Mariotto, M. Ferrari, Z. Crnjak Orel, A. Turković, K. Furić, J. Raman Spectrosc. 37 (2006) 161.
[35] P.G. Kuzmin, G.A. Shafeev, V.V. Bukin, S.V. Garnov, C. Farcau, R. Carles, B. Warot-Fontrose, V.G. Viau, J. Phys. Chem. C 114 (2010) 15266.